



OPEN

Theoretical study of the interaction of fullerenes with the emerging contaminant carbamazepine for detection in aqueous environments

Rodrigo A. Lemos Silva^{1✉}, Daniel F. Scalabrini Machado², Heibbe C. B. de Oliveira³, Luciano Ribeiro⁴ & Demétrio A. da Silva Filho¹

The global increase in drug consumption exposes the growing need to develop new systems for the detection, capture, and treatment of bioactive molecules. Carbamazepine is one instance of such contaminants at the top of the ranking commonly found in sewage treatment systems. This work, therefore, presents a theoretical study of fullerene C₆₀ and its derivatives with substitutional doping with B, Al, Ga, Si, Ge, N and P, for the detection and capture of carbamazepine in aqueous medium. Solvation effects were included by means of the Polarizable Continuum Solvent method. The results indicate that doped fullerenes are sensitive for the detection of carbamazepine both in gaseous and aquatic environments. Investigation on the intermolecular interactions between the drug and the fullerene molecule were carried out, allowing the characterization of the interactions responsible for stabilizing the adsorption of carbamazepine to the fullerenes. The theoretical survey revealed that fullerenes doped with Al, Ga, Si and Ge chemically adsorb carbamazepine whereas for the case of fullerenes doped with other heteroatoms physisorption is responsible for the molecular recognition. Relying on DFT calculations, the fullerene derivatives C₅₉Al, C₅₉Si and C₅₉Ga are the most suitable to act both as a sensor and to uptake carbamazepine in aquatic environments.

The rise in consumption of pharmaceuticals in health care in modern society has been accompanied by the lack of proper control of the fate of these substances in unutilized or metabolized forms^{1,2}. The persistence of these chemicals (the so-called emerging contaminants) in aquatic environment causes its accumulation and this process is on the rise posing potential harm to human health and aquatic biome as well. This alarming scenario urges for development of technologies to detect and treat pharmaceuticals at effluent treatment plants. One of the frequently detected pharmaceuticals in influents of wastewater treating plants^{3,4}, urban effluents⁵ and surface water⁵ is carbamazepine (CBZ), an anticonvulsant drug that is not very soluble in water^{6–8} and it is frequently deemed as one of the major pollutants of sewages^{8–11}.

Detection of emerging contaminants in the aqueous environment strongly depends on adsorption–desorption processes. Some conventional methods for detection of pharmaceuticals such as CBZ relies on the adsorption mechanism which is a multifactorial-dependent process. Some features are important for detection of contaminants such as surface properties of the adsorbent, type of solute (functional groups), chemical properties such as acidic or basic character, the size of the solute molecules, and types of interactions among species whether physical or electrostatic (Lewis acid–base reactions or oxidation)². Carbonaceous nanomaterials display some of these factors suitable for CBZ detection including carbon-nanotubes^{12,13}, carbon dots¹⁴ and fullerene (C₆₀)^{15,16}. C₆₀ can be a good choice for CBZ uptake because it provides a surface that is hydrophobic due to the size and curvature and is susceptible to interactions with its π -orbitals^{16,17} with the aromatic moiety of CBZ, enabling attractive dispersive and/or π -stacking interactions. Recently, Williams and coworkers performed adsorption studies using

¹Institute of Physics, University of Brasília, Brasília 70919-970, Brazil. ²Laboratório de Modelagem de Sistemas Complexos (LMSC), Instituto de Química, Universidade de Brasília, Brasília 70919-970, Brazil. ³Laboratório de Estrutura Eletrônica e Dinâmica Molecular (LEEDMOL), Instituto de Química, Universidade Federal de Goiás, Goiânia, Brazil. ⁴Grupo de Química Teórica e Estrutural de Anápolis, Campus de Ciências Exatas de Anápolis, Universidade Estadual de Goiás, Anápolis, Brazil. ✉email: silvarodrigo021@gmail.com

CBZ on colloids made of microplastics coated with C_{60} nanoclusters¹⁶, but contrastingly to other functionalized surfaces, the authors showed that CBZ uptake by C_{60} is negligible. This result indicates that non-polar pristine C_{60} surface does not bind CBZ effectively. Therefore, further decoration of the C_{60} surface with doping elements can enhance the intermolecular interactions between fullerene and CBZ. Indeed, doped-carbonaceous structures impart interesting features such as good physical–chemical sensitivity and high reactivity¹⁸, making fullerene-derivatives a frequent choice for both transport^{19–22} and drug detection^{18,23,24} applications.

During the last few years, carbon nanostructures have been the subject of several studies, from both theoretical and experimental standpoints. These studies paved the way for the development of several mechanisms for detection^{25–30}, storage and transport of various types of molecules^{31,32}. As reported by Saadat and Tavakol³³, for instance, theoretical calculations show that sulfur-doped-fullerenes boosts the surface adsorption of halogens and halides dramatically and this sensing improvement is affected by the inclusion of solvent effects (based on Polarizable Continuum models-PCM). Importantly, this work of Saadat and Tavakol shows that to elucidate specific binding interactions, further computational investigations is an invaluable approach to tackle the challenge of understanding adsorbent–contaminant interactions to aid the design of new sensors aiming at pharmaceutical detection in the environment.

In this context, the present work is dedicated to assessing the impact of doping fullerene with different elements in the adsorption energy aiming at CBZ uptake from theoretical calculations. Namely, $C_{59}X$ with $X = C, B, Al, Ga, Si, Ge, P$ and N were considered. These doping elements introduces electronic effects spanning from electron-deficient (B, Al and Ga atoms), electron-rich (N and P) and isoelectronic valence-shell (Si and Ge atoms) sites to elucidate how to increase the affinity of $C_{59}X$ with different regions of CBZ. A detailed study of electronic properties and the adsorption energies between the $C_{59}X$ -CBZ dimers were also performed. Since CBZ is a common pollutant found in aquatic environment, solvent effects were included in the present work, using the PCM-derived³⁴ solvation model.

Methodology and computational details

Geometric and electronic properties of the doped-fullerenes, CBZ and the respective dimers were determined under the framework of Density Functional Theory (DFT) employing the ω B97XD exchange–correlation functional coupled with the 6-31G(d) basis set. Pople-type of double- ζ quality 6-31G(d) basis set was employed for it being a suitable choice to deal with relatively large systems with a good compromise between accuracy and computational cost^{35–38} and it provides fairly good geometries and energetics when compared with experimental results, especially for large systems^{24,35,36,39–41}. Vibrational frequencies were calculated at the same level of theory to confirm that all structures correspond to genuine minima. These calculations were performed with the quantum chemistry Gaussian 09⁴² suite of programs. Solvent effects were included using the Polarizable Continuum Model (PCM)³⁴. Cartesian coordinates of the investigated species can be found in the Supplementary Information file, Tables S1, S2 and S3. The functional ω B97XD⁴³ is a long-range-corrected hybrid functional that includes Grimme’s empirical dispersion model D2⁴⁴, which adds an extra term to the energy obtained by DFT calculations. ω B97XD is a good choice to include London dispersion interactions which are crucial for the dimers studied here and shows good performance to treat non-covalent interactions³⁸. Besides that, our previously study showed that ω B97XD brings a good cost benefit for calculations involving molecular adsorption by fullerenes³⁷. Concerning HOMO–LUMO gap energies (E_g , HOMO-Highest Occupied Molecular Orbital and LUMO-Lowest Unoccupied Molecular Orbital), we selected M06L functional⁴⁵, relying on previous theoretical investigations revealing that this functional is suitable to predict the experimental value of E_g for the C_{60} fullerene¹⁸.

Adsorption energies (ΔE_{ads}) were computed within the supramolecular approach, in which the energy of the complex ($E_{complex}$) is subtracted from the energies of the monomers ($E_{CBZ} + E_{C_{59}X}$),

$$\Delta E_{ads} = E_{complex} - (E_{CBZ} + E_{C_{59}X}), \quad (1)$$

All energetics were corrected with the Basis Set Superposition Error (BSSE) using the counterpoise method⁴⁶.

Partial atomic charges were evaluated using ESP⁴⁷ charge analysis and from the molecular electrostatic potential (MEP) map of the systems were plotted.

To investigate the type of intermolecular interaction, Quantum Theory of Atom and Molecules (QTAIM)^{48–52} and Reduced Density Gradient (RDG) index^{53,54} were employed. Both approaches are based in the analysis of the electron density (ρ) and the second eigenvalue (λ_2) of the Hessian matrix ($\nabla^2\rho = \lambda_1 + \lambda_2 + \lambda_3$), at the called Bond Critical Points (BCPs) in the region between interacting molecules. QTAIM and RDG analysis has been applied to help categorizing non-covalent interactions in different systems^{33,55–57}. QTAIM and RDG properties were computed using the wavefunction analysis free program Multiwfn⁵⁸. The plot of the isosurfaces and molecules for both QTAIM and RDG analysis were made with VMD software version 1.9.3⁵⁹.

Results and discussion

Doping effects on the frontier orbitals. To investigate the electronic properties of the $C_{59}X$ fullerenes, we employed the M06L/6-31G(d)// ω B97XD/6-31G(d) model. The M06L exchange–correlation functional is well-suited to predict HOMO–LUMO gap energies¹⁸ in close agreement with the experimental E_g values ranging from 1.80⁶⁰ up to 1.90 eV⁶¹ in the case of pristine fullerene (see Table 1).

The C_{60} Highest Occupied Molecular Orbital (HOMO) showed quintuple degeneration and the Lowest Occupied Molecular Orbital (LUMO) showed a triple degeneration. As already observed in previous studies⁶², C_{60} doping tends to break this degeneration. The reduction of the energy gap between the border orbitals is recurrently observed in doped carbon nanostructures^{19,21,24,63–66}. The results obtained for the $C_{59}X$ confirm this trend. Glancing at Table 1 and Fig. 1, it can be observed that, in general, the $C_{59}X$ exhibited a decrease in the energy

Molecules	M06L/6-31G(d)							
	Vacuum				Water			
	E_H	E_L	E_g	ΔE_g	E_H	E_L	E_g	ΔE_g
CBZ	-5.270	-1.865	3.405	-	-5.486	-1.957	3.529	-
C ₅₉ B	-5.219	-3.637	1.583	-16.855	-5.103	-3.518	1.585	-16.731
C ₅₉ Al	-4.960	-3.499	1.461	-23.245	-4.847	-3.428	1.419	-25.411
C ₅₉ Ga	-5.011	-3.539	1.472	-22.674	-4.891	-3.449	1.442	-24.210
C ₆₀	-5.542	-3.638	1.903	-	-5.420	-3.517	1.903	-
C ₅₉ Si	-5.381	-3.989	1.392	-26.862	-5.233	-3.835	1.398	-26.541
C ₅₉ Ge	-5.313	-4.083	1.230	-35.397	-5.293	-3.963	1.331	-30.073
C ₅₉ P	-4.776	-3.660	1.116	-41.358	-4.776	-3.659	1.118	-41.270
C ₅₉ N	-4.268	-3.704	0.564	-70.364	-4.123	-3.572	0.552	-71.000

Table 1. Energies (in eV) of the frontier orbitals and HOMO–LUMO gap for the doped fullerenes and its percentual variation upon complexation of CBZ (ΔE_g in%) as determined at the M06L/6-31G(d)//wB97XD/6-31G(d) level of theory.

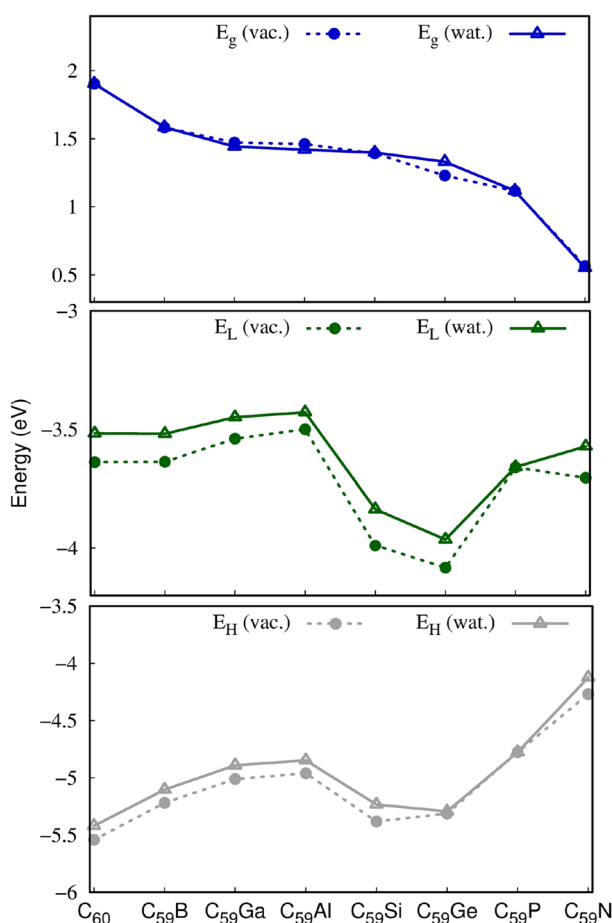


Figure 1. Frontier orbital energies and HOMO–LUMO orbital energy gap of the doped fullerenes as determined at the M06/6-31G(d)//wB97XD/6-31G(d) level of theory in vacuum and water (PCM).

gap, E_g , relative to the C₆₀ fullerene in both vacuum and water. Figure 1 also portrays the marginal impact of the implicit solvation treatment on the energies of the frontier states and the energy gaps.

The value of E_g can be adopted as an index of chemical stability, so that lower values of E_g is commonly associated with higher reactivity⁶⁷. Thus, the energetic variation of frontier orbitals indicates an increase in chemical sensitivity of heterofullerenes⁶³. The decreasing order of E_g can be observed in Fig. 1 and this trend was ubiquitous for all doped fullerenes regardless of environment. Moreover, it can be observed that the reduction of E_g in C₅₉X, is more strongly influenced by the increase of orbital HOMO energy, i.e., E_H , destabilizes whereas E_L , was

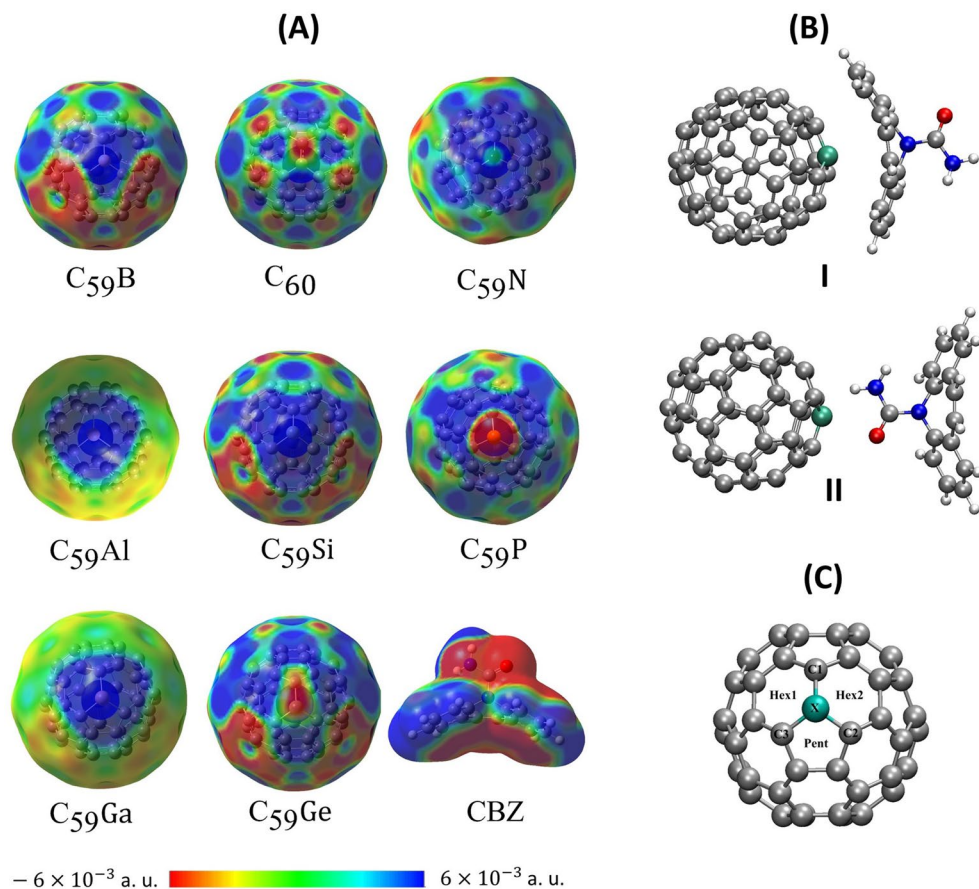


Figure 2. (A) $C_{59}X$ Molecular Electrostatic Potential in the range of $\pm 6 \times 10^{-3}$ a. u. (B) Initial relative orientations for the $C_{59}X$ -CBZ dimers. (C) Frontal view of the doping atom X, highlighting the surrounding carbons and hexagonal and pentagonal faces around the heteroatom.

nearly constant for all different dopants, except for $C_{59}Si$ and $C_{59}Ge$, in line with previous studies for doped C_{60} fullerenes obtained with B3LYP/6-31G(d)⁶⁸. E_H increases in the following order: C_{60} , $C_{59}Ge$, $C_{59}Si$, $C_{59}B$, $C_{59}Ga$, $C_{59}Al$, $C_{59}P$ and $C_{59}N$, indicating that the electronic perturbation of the system, either by of electron rich or deficient-elements in the C_{60} valence shell, produces destabilization of the HOMO orbital.

For the elements of group 13, the insertion of the heteroatoms generates an electronic vacancy in the HOMO orbital. Hence, the formation of a Singly Occupied Molecular Orbital (SOMO) with higher energy than the C_{60} HOMO orbital occurs^{62,69,70}. The new SOMO orbital is positioned energetically above the HOMO orbital of neat fullerene. In the case of N- and P-doping, which has one extra electron in the valence shell, also leads to the formation of a new SOMO orbital⁶⁹⁻⁷¹, which is also energetically positioned above of the HOMO orbital of pristine fullerene. For the $C_{59}Si$ and $C_{59}Ge$, since they are isoelectronic in the valence-shell to the carbon atom, HOMO was less affected by the doping element (see lower panel of Fig. 1). For these elements the E_g reduction is attributed by the more important decrease in E_L . Such effect was already reported in the literature^{18,63,68,72}.

MEP and ESP partial atomic charges. Figure 2A brings the molecular electrostatic potential (MEP) maps for the doped fullerenes. Table S4 shows the values of ESP charges of the heteroatoms of each $C_{59}X$ structure.

For doped fullerenes, with B, Al, Ga and Si, an electrophilic behavior was observed in the region around the doping atom, as can be seen in Fig. 2A. For the fullerenes doped with Ge, N and P, one can see a nucleophilic behavior over the dopant atoms with charge accumulation. It is also possible to note a positive charge region in the carbons near the Ge, N and P atoms. Through the MEPs for the doped fullerenes, it is observed that the heteroatom generates a significant non-local electronic perturbation over the fullerene cage. It is also noted that, around the dopant, there is an electrophilic region with can represent an important site for interaction with CBZ. Still looking at Fig. 2A, it is noted that the drug has a reactive region in the amide group and in the below the aromatic rings opposite to the amide moiety displaying nucleophilic behavior. In view of the predominantly electrophilic characteristics of doped fullerenes, it is assumed, therefore, that the CBZ molecule will have a greater tendency to interact with $C_{59}X$ along the carbonyl fragment.

Inspired by the MEPS displayed in Fig. 2A, we performed the optimization of the complexes $CBZ + C_{59}X$ considering two configurations of the CBZ molecule as displayed in Fig. 2B. The configuration (I) was considered,

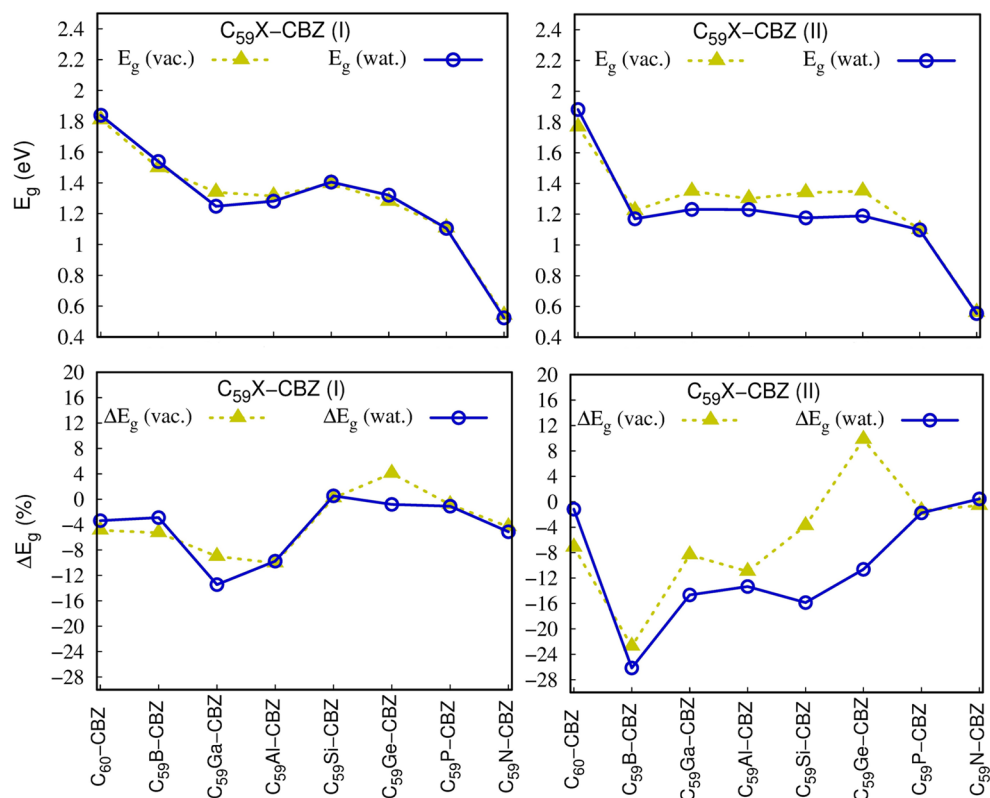


Figure 3. (Top panel) HOMO–LUMO gap energy (E_g) of $C_{59}X$ in the complex configuration ($C_{59}X + CBZ$) in vacuum and water (PCM) and (lowest panel) percentual change of E_g (ΔE_g) with respect to its value prior to the CBZ adsorption. These calculations were performed at the M06L/6-31G(d)//wB97XD/6-31G(d) level of theory.

observing the largest superficial area of the aromatic fragments to establish interactions between the fullerenes and the drug. Thus, it is expected both configurations will display non-negligible interactions and hence, configurations (I) and (II) were conducted in this work.

Frontier orbitals energy variations upon complexation of CBZ. The sensing capability of doped fullerenes for CBZ adsorption was studied by considering the variation of E_g after the adsorption of CBZ. Figure 3 depicts the effect of doping and interaction with CBZ of the E_g and the percentage variation of the gap, ΔE_g , which measures the percentage variation of E_g of the $C_{59}X$ after the CBZ adsorption on the fullerene cage (Table S5 present the numerical values of E_H , E_L , E_g and ΔE_g). The change of the E_g is an important parameter, since the energy gap is directly correlated with electrical conductivity (σ), $\sigma \propto \exp(-E_g/2k_B T)^{73}$ (T is the temperature, and k_B represents Boltzmann constant) so that if the E_g of the doped-fullerene is strongly affected by the presence of CBZ an electronic signal enables identification of the drug.

Figure 3 (top panel) portrays interesting features, such as, (i) similar to that observed in the case of isolated $C_{59}X$, dopants decreases the E_g gap (recall Fig. 1), (ii) PCM solvation treatment exhibit little impact on E_g to order of ~ 0.1 eV, and (iii) the relative orientation of CBZ with respect to the doped site on fullerene, the relative configurations I and II, display significant differences only when the doping atom is B, Si and to a lesser extent Ge. To assess more profoundly the changes of E_g when $C_{59}X$ interacts with CBZ, we can see from Fig. 3 (lowest panel), for configuration II in water, that the doping atoms B, Ga, Al, Si and Ge provokes large variations of the E_g gap, that is, from an electronic standpoint, these heterofullerenes show more sensibility towards CBZ. Still focusing on Fig. 3 (lowest panel), we note that dopants N, P and Ge, the variation of the E_g gap after complexation in vacuum, was positive, that is the interaction actually increased the gap afterwards complexation especially in configuration II (positive values of ΔE_g). These effects might be attributed to electrostatic repulsions between the polar amide fragment of CBZ and the electron-rich dopants in $C_{59}X$ as discussed in the MEPs presented in Fig. 2.

Adsorption energies in gas and aqueous phase. Because $\omega B97XD$ is reported to deliver good interaction energies between system where non-covalent interactions are important^{37,38,72,74,75}, we will henceforth discuss the interaction energies between CBZ and $C_{59}X$ relying on calculations performed at the $\omega B97XD/6-31G(d)$ level of theory. In Table 2 and Fig. S2, the results for the adsorption energy between the $C_{59}X$ molecules and the CBZ are presented for both vacuum and aqueous environments and were BSSE-corrected. The pristine C_{60} showed the smallest adsorption energy in both configurations and environments. In general, the doping effect was to increase (in modulus) the ΔE_{ads} energy. Solvation effects had little impact on ΔE_{ads} , but for most complexes the interaction was enhanced in water environment.

Systems	Vacuum				Water	
	(ev)					
	Conf	BSSE	ΔE_{ads}	$\Delta E_{ads}(BSSE)$	ΔE_{ads}	$\Delta E_{ads}(BSSE)$
C ₅₉ B-CBZ	I	0.161	-0.736	-0.576	-0.701	-0.540
	II	0.241	-1.572	-1.331	-1.562	-1.321
C ₅₉ Al-CBZ	I	0.206	-1.423	-1.218	-1.600	-1.395
	II	0.247	-2.658	-2.411	-2.944	-2.697
C ₅₉ Ga-CBZ	I	0.642	-1.603	-0.961	-1.748	-1.106
	II	0.566	-2.398	-1.831	-2.312	-1.745
C ₆₀ -CBZ	I	0.159	-0.683	-0.524	-0.656	-0.497
	II	0.086	-0.266	-0.180	-0.431	-0.345
C ₅₉ Si-CBZ	I	0.152	-0.738	-0.585	-0.700	-0.548
	II	0.267	-2.191	-1.924	-2.223	-1.956
C ₅₉ Ge-CBZ	I	0.741	-1.303	-0.563	-1.483	-0.742
	II	0.667	-1.863	-1.196	-1.934	-1.267
C ₅₉ N-CBZ	I	0.153	-0.718	-0.565	-0.667	-0.514
	II	0.131	-0.515	-0.384	-0.436	-0.305
C ₅₉ P-CBZ	I	0.173	-0.740	-0.567	-0.686	-0.513
	II	0.156	-0.543	-0.387	-0.512	-0.355

Table 2. Adsorption energy, ΔE_{ads} , with and without BSSE correction for the interaction between CBZ and C₅₉X fullerenes as determined at the ω B97XD /6-31 g(d) level of theory. Solvation effects were included by means of the Polarizable Continuum Model.

As can be observed in the optimized systems presented in Fig. S1 and in previous studies^{21,24,62,63}, C₆₀ doping generates a structural deformation localized in the region of the heteroatom. Thus, it is plausible to assume that the atomic radius of the X atom influences the order of interaction between the C₅₉X and the CBZ. An estimate for the atomic radius, of the heteroatoms, can be obtained through the medium variation of the bonds between the neighboring carbons to the dopant atom.

Due to the larger atomic radius, the atoms of Al, Ga, Ge, Si, P and B are projected outside of the C₅₉X structure, which makes these heteroatoms more susceptible to nucleophilic/electrophilic attacks. This heteroatom projection can be observed by the variation of the bond length between the carbon atoms and the X atom. Table S4 presents the atomic radius⁷⁶, R_{α} , of the heteroatoms in the doped fullerene and the average bond length, R_{ave} , between the heteroatoms and the surrounding carbon atoms. The R_{ave} values obtained here agree with values obtained in previous studies^{63,68}. Through the data presented in Table S4, it can be noted that the order of interaction, tends to follow the increasing order of R_{α} and R_{ave} . However, it is important to point out that, the electronic behavior of the C₅₉X also may influence the interaction with CBZ.

Although the systems doped with P and Ge presented larger R_{α} and R_{ave} , the nucleophilic behavior of the C₅₉Ge and C₅₉P, at the doping site, may explain the higher value of ΔE_{ads} obtained for others C₅₉X-CBZ in comparison with the values of ΔE_{ads} obtained for C₅₉Ge-CBZ and C₅₉P-CBZ. Besides that, it is also possible to note that, although Al and Ga present very similar R_{α} and R_{ave} values, Al atom has a higher ESP charge than Ga atom, as presented in Table S4. For this reason, the ΔE_{ads} is larger for C₅₉Al than C₅₉Ga. For both configurations, C₅₉X interact with nucleophilic regions of CBZ. Therefore, it is expected that systems with more electrophilic characteristics, around the X atom, and with higher R_{α} and R_{ave} values, have a better interaction with CBZ. Thus, because of the more electrophilic behavior, presented in Fig. 1 and Table S4, and due the large value of R_{α} and R_{ave} , the C₅₉Al system presents a higher interaction with CBZ in both, gas and aqueous environment.

However, an interesting exception to this tendency can be observed for the ΔE_{ads} obtained by C₅₉Ga and C₅₉Si, in conf. II and in both phases. Although Ga presented higher ESP charge, R_{α} and R_{ave} values, C₅₉Si presents higher ΔE_{ads} than C₅₉Ga. In order to understand this exception, the charge distribution, along the hexanes and pentane face surrounding the heteroatoms, was evaluated. It is well known that dominant partial charges, either positive or negative, accumulated on specific parts of interacting molecules have important influence for effective interaction^{74,77,78}. Bearing it in mind, the sum of the ESP charges in the two hexanes faces and in the pentane face around the doping atoms was taken into account (See Fig. 2C). These results are presented in Table S4. By means of these data, it was observed that, the C₅₉Si has the highest positive value of the total charge in the pentane face. For this reason, CBZ reoriented to interact specially with this face. This pentane-CBZ interaction is responsible for increasing of ΔE_{ads} . This interaction, together with a possible electrostatic dipolar bond, discussed in more details in “Non-covalent interaction” section, would be enough to stabilize C₅₉Si when compared to C₅₉Ga.

To clarify the nature of these interactions in the C₅₉X-CBZ systems, a detailed study of the intermolecular interactions, in both configurations and phases, was carried out.

Non-covalent interactions. To investigate the nature of the interaction between doped fullerenes and the CBZ drug, the Reduced Density Gradient (RDG), together with Quantum Theory of Atoms in Molecules

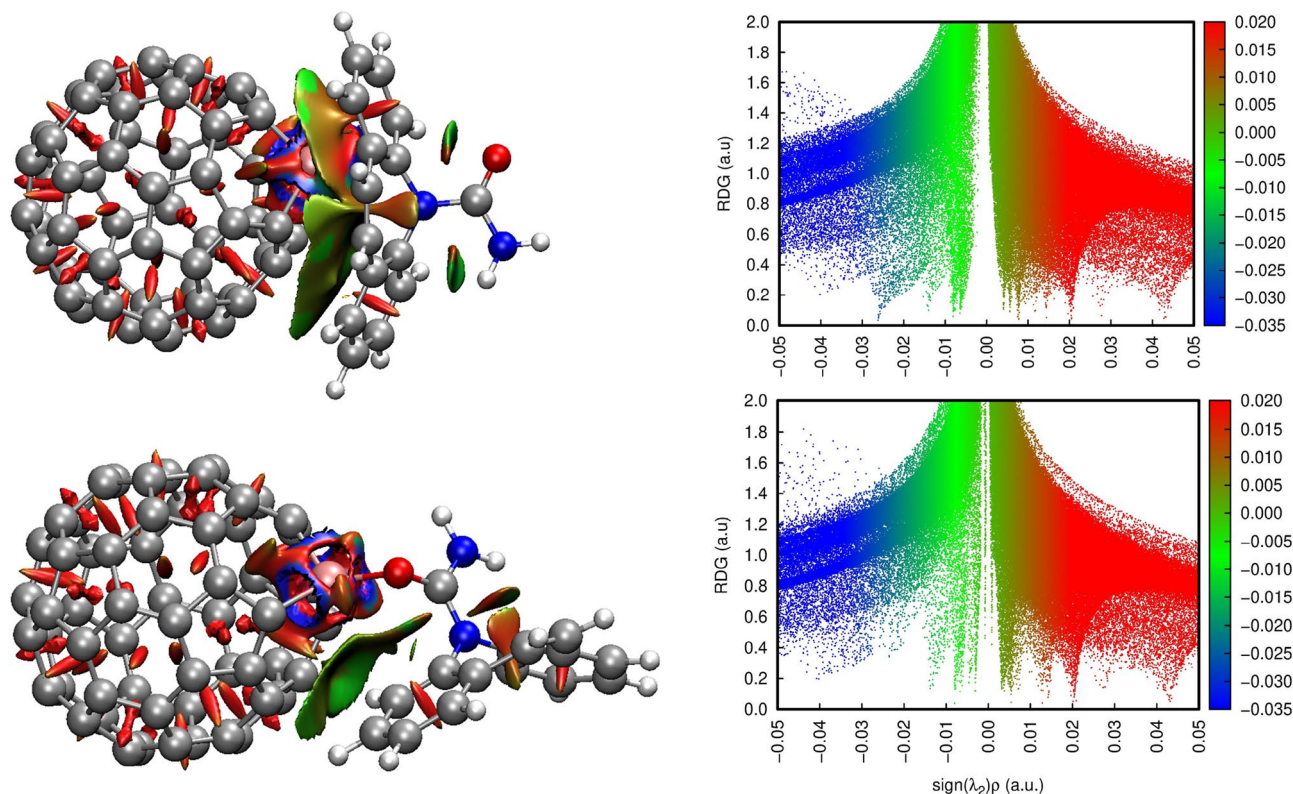


Figure 4. RDG isosurfaces and scatter graphs for $C_{59}Al$ -CBZ (I) (top) and $C_{59}Al$ -CBZ (II) (bottom). Red-colored regions indicate a repulsive force, green-colored regions indicated van der Waals interactions and blue-colored regions indicated strong attractive non-covalent interaction.

(QTAIM) were employed. In the RDG analysis, the combination of electron density ρ and the signal of λ_2 provides a tool to distinguish between repulsive or attractive interactions. For this task, the function $sign(\lambda_2)\rho$ is defined as a product of signal of λ_2 with ρ . While more negatives values of $sign(\lambda_2)\rho$ indicate attractive interactions (represented by blue surfaces), such as hydrogen bonds or dipole–dipole interactions, positive values are attributed to nonbonding interactions (red surfaces). Values of $sign(\lambda_2)\rho$ close to zero (green surfaces), are attributed to van der Waals (vdW) interactions^{53,54}. For details of RDG analysis and QTAIM properties the reader is referred to refs^{33,78–81}.

Tables S6, S7, S8 and S9 summarize the QTAIM results for both phases. The BCPs (Bond Critical Points), in Tables S8 and S9, are represented by orange points and the bond paths by the yellow lines. By means of the data presented in Tables S6–S9, one can see that, according to the QTAIM scheme, in configuration (I) almost all systems presented van der Waals interaction. The exceptions were observed for Al and Ga which presented interactions with character resembling polar covalent bonds, in both gas and aqueous phase.

For $C_{59}Al$ -CBZ (II), in both phases, the values observed in Tables S6 and S7 indicate that an interaction with ionic character was observed between Al and O from CBZ. For $C_{59}B$ -CBZ (II), $C_{59}Ga$ -CBZ (II), $C_{59}Si$ -CBZ (II) and $C_{59}Ge$ -CBZ (II), in both phases, a partial covalent character interaction was observed between the heteroatom and the oxygen in CBZ. For the C_{60} -CBZ (II) $C_{59}P$ -CBZ (II) and $C_{59}N$ -CBZ (II), for both phases, QTAIM parameters indicate that the intermolecular interactions for these complexes are exclusively of van der Waals type.

As mentioned before, the N and P dopants, in $C_{59}N$ and $C_{59}P$, have a nucleophilic character which induces a reorientation of CBZ in front of the fullerene cage. Tables S8 and S9 present the optimized structure, in gas phase and aqueous environment respectively, where it can be seen this CBZ reorientation. For this reason, the CBZ in $C_{59}N$ -CBZ and $C_{59}P$ -CBZ, prefers interacting to the fullerene cage instead to the dopant atoms. The CBZ reorientation was observed in both phases and configurations. This may explain the exclusivity of van der Waals interaction in these complexes.

Additionally, in gas phase, for $C_{59}Si$ and $C_{59}Ge$, one $C \cdots H$ electrostatic dipolar bonding was observed in each one of these systems. As discussed in the “Adsorption energies in gas and aqueous phase” section, this electrostatic dipolar $C \cdots H$ bonding (See values of BCP 1 for Conf. II at Tables S6 and S7 for $C_{59}Si$ -CBZ) together to the ESP accumulation charge, would help to explain the increase in the stabilization for $C_{59}Si$ -CBZ, comparing with the stabilization energy of $C_{59}Ga$ -CBZ (See Fig. 2 and Table 2). For $C_{59}Ge$ -CBZ, the value of ΔE_{ads} is affected by the nucleophilic character of Ge atom in the fullerene cage (See Table S4). For this reason, the $C \cdots H$ electrostatic dipolar bonding does not produce a notable increase in the stabilization of $C_{59}Ge$ -CBZ system.

Now focusing on RDG analyses, the isosurfaces were associated with the scattering graphs, shown in Fig. 4 and Tables S8 and S9. In Fig. 4 the RDG isosurfaces and the scatter graph for $C_{59}Al$ -CBZ is presented. Green-colored isosurfaces indicate non-covalent interactions while red-ones is due to steric effects. The blue-colored

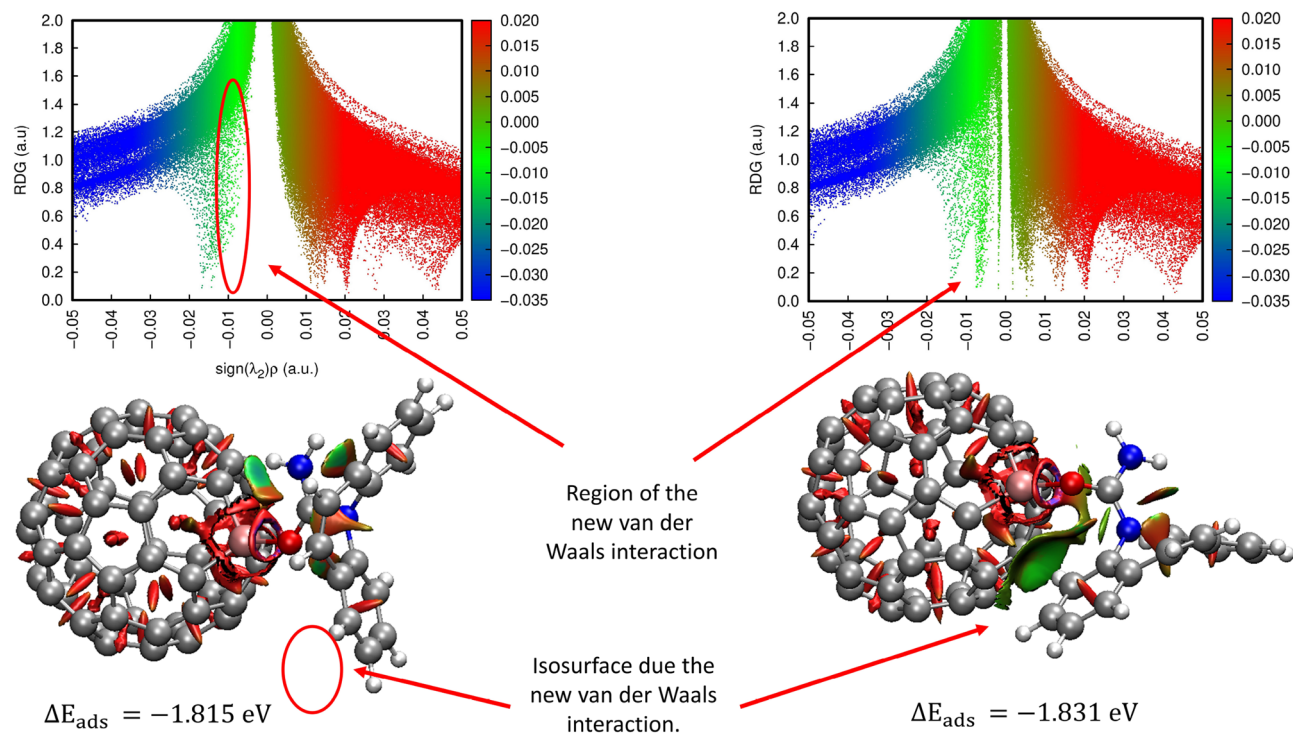


Figure 5. RDG isosurfaces and scatter graphs for the two local minima configuration of $C_{59}\text{Ga-CBZ (II)}$. On the left, a local minimal structure presents the lack of a vdW interaction. On the right, after a new scan calculation, the missed vdW interaction appears. This new vdW interactions helps in a slight increase of the ΔE_{ads} .

regions represent strong attractive effects. The RDG isosurfaces and scatter graph for all $C_{59}\text{X-CBZ}$ complexes are detailed in Tables S8 and S9.

For the $C_{59}\text{B-CBZ}$ and $C_{59}\text{N-CBZ}$ complexes, in both phases and configurations, the RDGs isosurfaces and scatter graphs are similar to the RDGs surfaces and scatter graphs observed for $C_{60}\text{-CBZ}$. This may be due the heteroatom radius. B and N have R_{α} close to carbon, the fullerene cage is less deformed and the contact area for vdW interactions is similar to the case of pristine fullerene. On another hand, it was observed that the scatter graph presented more points in the attractive region for $C_{59}\text{Al-CBZ (I)}$, $C_{59}\text{Si-CBZ (I)}$, $C_{59}\text{Ga-CBZ (I)}$ and $C_{59}\text{Ge-CBZ (I)}$, in both phases. Again, it is observed that for those larger heteroatoms NCI increases accordingly. These observations are in line with the interaction strength order of the $C_{59}\text{X-CBZ}$ complexes.

For these systems in conf. (II), QTAIM results indicated that the heteroatom-oxygen interaction may have a greater importance for ΔE_{ads} . However, as showed for both, QTAIM and RDG, NCIs still play a significant role in the stabilization of the systems, especially for $C_{59}\text{Al-CBZ (II)}$, which has an important vdW interaction in the green region of the RDG isosurfaces (see BCPs 2 in Tables S6, S7, S8, S9 and Fig. 4), and for $C_{59}\text{Si-CBZ}$ and $C_{59}\text{Ge-CBZ (II)}$, which have an indication of an electrostatic interaction (see BCPs 1 in Tables S6 and S8).

By means of non-covalent interaction analyses, it was observed that, for all complexes in configuration (I), and for $C_{60}\text{-CBZ (II)}$, $C_{59}\text{P-CBZ (II)}$ and $C_{59}\text{N-CBZ (II)}$, the drug is physisorbed to the fullerene cage. Nevertheless, for $C_{59}\text{Al-CBZ (II)}$, $C_{59}\text{B-CBZ (II)}$, $C_{59}\text{Ga-CBZ (II)}$, $C_{59}\text{Ge-CBZ (II)}$ and $C_{59}\text{Si-CBZ (II)}$, a chemical interaction occurs between CBZ and these doped fullerenes. We should note, however, that $C_{59}\text{Ga-CBZ (II)}$ exhibited another local minimum, and this configuration is presented in Fig. 5.

Aiming to find the true minimal structure for $C_{59}\text{Ga-CBZ (II)}$ a relaxed scan was made having as starting point the structure presented at the left of Fig. 5. For this relaxed scan, we rotated the CBZ in front of the $C_{59}\text{Ga}$, making a variation of 10° for each position. All 36 calculations converged to the structure presented at the right in Fig. 5 which indicated that this is the true minimal configuration for $C_{59}\text{Ga-CBZ (II)}$.

One can see that, comparing this local minimum region to the global minimum region, the presence of an extra vdW interaction helped in the increase of ΔE_{ads} in 0.016 (eV). This small increase in the energy confirms that the interaction between the Ga atom to the O atom from CBZ may represent the major influence for the ΔE_{ads} in the $C_{59}\text{Ga-CBZ (II)}$. However, besides these new stable configurations, it is important to highlight that, due the small energy difference in the ΔE_{ads} , these possible new configurations, for $C_{59}\text{X-CBZ (II)}$, may not have influence on the CBZ adsorption capacity presented by the $C_{59}\text{X}$ molecules. The results indicate that, due their ΔE_{ads} values and electrophilic character, $C_{59}\text{Al}$, $C_{59}\text{Si}$ and $C_{59}\text{Ga}$ are the doped fullerenes more indicated for acting as both, sensor, and capture system of carbamazepine.

Conclusions

The main purpose of this study is to investigate the adsorption of carbamazepine in pristine and doped fullerenes to disclose its capability to sense this drug. Two relative orientations of CBZ with respect to the doping site were considered. Frontier orbital analysis showed that the HOMO–LUMO energy gap decreases whether employing heteroatoms from group 13, 14 or 15. Solvation effects modelled by means of the PCM approach had little impact on electronic, geometric, and energetic properties. Upon complexation, it was observed a gap variation in almost all $C_{59}X$ -CBZ systems. In water, almost all complexes showed a gap reduction after the CBZ interaction. The results indicated that this gap variation would produce a signal due to changes in electrical conductivity of doped fullerene when CBZ adsorbs. The adsorption energies were enhanced for every heteroatom, but the most stable complex was obtained with Al-doping. Group 15 elements do not stabilize the complexes significantly and therefore, are not suitable to detect organic structures with polar functional groups such as the amide fragment of CBZ. Intermolecular interaction analyses were conducted within the framework of the QTAIM descriptors. It was observed that a chemical interaction occurs for $C_{59}Al$ -CBZ (II), $C_{59}B$ -CBZ (II), $C_{59}Ga$ -CBZ (II), $C_{59}Ge$ -CBZ (II) and $C_{59}Si$ -CBZ (II). Almost all these complexes presented a partial covalent character interaction between the doping atom and the oxygen in CBZ molecule. The exception was observed for $C_{59}Al$ -CBZ (II), which presented an ionic character interaction between the Al atom, from $C_{59}Al$, and the O atom, from CBZ. For all complexes in configuration (I), and for C_{60} -CBZ (II), $C_{59}P$ -CBZ (II) and $C_{59}N$ -CBZ (II), the drug has a physis adsorption. The cage structural and electronic deformation was evaluated to understand the interaction order. It was observed that, for those doped fullerenes with higher local structural deformation and higher electrophilic character, the drug adsorption was favored. In another word, the interaction order follows the heteroatom size and the electrophilic behavior around the doping region. This was corroborated by the analysis of NCI. Our calculations showed that $C_{59}Al$ -CBZ (II) presented the highest value for ΔE_{ads} with, -2.411 eV in gas phase and -2.697 eV in aqueous media. Finally, our results indicate that, due their greatest adsorption energy, in both phases and configurations, $C_{59}Al$, $C_{59}Ga$ and $C_{59}Si$ are potential candidates aiming at drug sensor applications.

Data availability

The data presented in this study are available in the article and in the Supporting Information file.

Received: 21 February 2022; Accepted: 26 August 2022

Published online: 23 September 2022

References

- Drillia, P. *et al.* On the occasional biodegradation of pharmaceuticals in the activated sludge process: The example of the antibiotic sulfamethoxazole. *J. Hazard. Mater.* **122**, 259–265 (2005).
- Akhtar, J., Amin, N. A. S. & Shahzad, K. A review on removal of pharmaceuticals from water by adsorption. *Desalin. Water Treat.* **57**, 12842–12860 (2016).
- Castiglioni, S. *et al.* Removal of pharmaceuticals in sewage treatment plants in Italy. *Environ. Sci. Technol.* **40**, 357–363 (2006).
- Spongberg, A. L. & Witter, J. D. Pharmaceutical compounds in the wastewater process stream in Northwest Ohio. *Sci. Total Environ.* **397**, 148–157 (2008).
- Kim, S. D., Cho, J., Kim, I. S., Vanderford, B. J. & Snyder, S. A. Occurrence and removal of pharmaceuticals and endocrine disruptors in South Korean surface, drinking, and waste waters. *Water Res.* **41**, 1013–1021 (2007).
- Borisover, M., Sela, M. & Chefetz, B. Enhancement effect of water associated with natural organic matter (NOM) on organic compound-NOM interactions: A case study with carbamazepine. *Chemosphere* **82**, 1454–1460 (2011).
- Zerrouk, N., Chemtob, C., Arnaud, P., Toscani, S. & Dugue, J. In vitro and in vivo evaluation of carbamazepine-PEG 6000 solid dispersions. *Int. J. Pharm.* **225**, 49–62 (2001).
- Zhang, Y., Geißen, S. U. & Gal, C. Carbamazepine and diclofenac: Removal in wastewater treatment plants and occurrence in water bodies. *Chemosphere* **73**, 1151–1161 (2008).
- Huang, Y., Guo, J., Yan, P., Gong, H. & Fang, F. Sorption-desorption behavior of sulfamethoxazole, carbamazepine, bisphenol A and 17 α -ethinylestradiol in sewage sludge. *J. Hazard. Mater.* **368**, 739–745 (2019).
- Martínez-Alcalá, I., Pellicer-Martínez, F. & Fernández-López, C. Pharmaceutical grey water footprint: Accounting, influence of wastewater treatment plants and implications of the reuse. *Water Res.* **135**, 278–287 (2018).
- Mohapatra, D. P., Brar, S. K., Tyagi, R. D., Picard, P. & Surampalli, R. Y. Analysis and advanced oxidation treatment of a persistent pharmaceutical compound in wastewater and wastewater sludge-carbamazepine. *Sci. Total Environ.* **470–471**, 58–75 (2014).
- Lerman, I., Chen, Y., Xing, B. & Chefetz, B. Adsorption of carbamazepine by carbon nanotubes: Effects of DOM introduction and competition with phenanthrene and bisphenol A. *Environ. Pollut.* **182**, 169–176 (2013).
- Oleszczuk, P., Pan, B. & Xing, B. Adsorption and desorption of oxytetracycline and carbamazepine by multiwalled carbon nanotubes. *Environ. Sci. Technol.* **43**, 9167–9173 (2009).
- Deng, Y., Ok, Y. S., Mohan, D., Pittman, C. U. & Dou, X. Carbamazepine removal from water by carbon dot-modified magnetic carbon nanotubes. *Environ. Res.* **169**, 434–444 (2019).
- Kalanur, S. S., Jaldappagari, S. & Balakrishnan, S. Enhanced electrochemical response of carbamazepine at a nano-structured sensing film of fullerene-C60 and its analytical applications. *Electrochim. Acta* **56**, 5295–5301 (2011).
- Williams, T., Walsh, C., Murray, K. & Subir, M. Interactions of emerging contaminants with model colloidal microplastics, C60 fullerene, and natural organic matter: Effect of surface functional group and adsorbate properties. *Environ. Sci. Process. Impacts* **22**, 1190–1200 (2020).
- Keiluweit, M. & Kleber, M. Molecular-level interactions in soils and sediments: The role of aromatic π -systems. *Environ. Sci. Technol.* **43**, 3421–3429 (2009).
- Hazrati, M. K. & Hadipour, N. L. Adsorption behavior of 5-fluorouracil on pristine, B-, Si-, and Al-doped C60 fullerenes: A first-principles study. *Phys. Lett. Sect A Gen. At. Solid State Phys.* **380**, 937–941 (2016).
- Esfahli, M. D. & Janebi, H. B-, N-doped and BN codoped C60 heterofullerenes for environmental monitoring of NO and NO₂: A DFT study. *Mol. Phys.* **118**, 1–9 (2020).
- Hadipour, N. L., Ahmadi Peyghan, A. & Soleymanabadi, H. Theoretical study on the Al-doped ZnO nanoclusters for CO chemical sensors. *J. Phys. Chem. C* **119**, 6398–6404 (2015).
- Esfahli, M. D. & Heydari, S. C 59 X heterofullerenes (X=N, B, Si, P and S) as catalysts for reduction of N₂O: A comparative DFT study. *ChemistrySelect* **4**, 2267–2274 (2019).

22. Vessally, E., Siadati, S. A., Hosseinian, A. & Edjlali, L. Selective sensing of ozone and the chemically active gaseous species of the troposphere by using the C20 fullerene and graphene segment. *Talanta* **162**, 505–510 (2017).
23. Hosseinian, A., Vessally, E., Yahyaei, S., Edjlali, L. & Bekhradnia, A. A density functional theory study on the interaction between 5-fluorouracil drug and C24 fullerene. *J. Clust. Sci.* **28**, 2681–2692 (2017).
24. Moradi, M., Nouraliei, M. & Moradi, R. Theoretical study on the phenylpropanolamine drug interaction with the pristine, Si and Al doped [60] fullerenes. *Phys. E Low-Dimensional Syst. Nanostruct.* **87**, 186–191 (2017).
25. Yang, C. M. *et al.* Ultraviolet illumination effect on monolayer graphene-based resistive sensor for acetone detection. *Vacuum* **140**, 89–95 (2017).
26. Nomani, M. W. K. *et al.* Highly sensitive and selective detection of NO₂ using epitaxial graphene on 6H-SiC. *Sensors Actuators B Chem.* **150**, 301–307 (2010).
27. Romero, H. E. *et al.* Adsorption of ammonia on graphene. *Nanotechnology* **20**, 245501 (2009).
28. Justino, C. I. L., Gomes, A. R., Freitas, A. C., Duarte, A. C. & Rocha-Santos, T. A. P. Graphene based sensors and biosensors. *TrAC Trends Anal. Chem.* **91**, 53–66 (2017).
29. Feng, X. *et al.* Three-dimensional nitrogen-doped graphene as an ultrasensitive electrochemical sensor for the detection of dopamine. *Nanoscale* **7**, 2427–2432 (2015).
30. Li, X. *et al.* Electrochemical sensing of nicotine using screen-printed carbon electrodes modified with nitrogen-doped graphene sheets. *J. Electroanal. Chem.* **784**, 77–84 (2017).
31. Vijayaraghavan, V., Dethan, J. F. N. & Garg, A. Nanomechanics and modelling of hydrogen stored carbon nanotubes under compression for PEM fuel cell applications. *Comput. Mater. Sci.* **146**, 176–183 (2018).
32. Reina, M., Celaya, C. A. & Muñoz, J. C36 and C35E (E=N and B) fullerenes as potential nanovehicles for neuroprotective drugs: A comparative DFT study. *ChemistrySelect* **6**, 4844–4858 (2021).
33. Saadat, K. & Tavakol, H. An exceptional functionalization of doped fullerene observed via theoretical studies on the interactions of sulfur-doped fullerenes with halogens and halides. *RSC Adv.* **5**, 55227–55237 (2015).
34. Mennucci, B. Polarizable continuum model. *Wiley Interdiscip. Rev. Comput. Mol. Sci.* **2**, 386–404 (2012).
35. Zandler, M. E. & D'Souza, F. The remarkable ability of B3LYP/3-21G(*) calculations to describe geometry, spectral and electrochemical properties of molecular and supramolecular porphyrin-fullerene conjugates. *Comptes Rendus Chim.* **9**, 960–981 (2006).
36. Stephens, P. J., Devlin, F. J., Chabalowski, C. F. & Frisch, M. J. Ab Initio calculation of vibrational absorption and circular dichroism spectra using density functional force fields. *J. Phys. Chem.* **98**, 11623–11627 (1994).
37. Silva, L. *et al.* Harnessing greenhouse gases absorption by doped fullerenes with externally oriented electric field. *Molecules* **27**, 2968 (2022).
38. Silva, R. A. L. *et al.* The influence of the configuration of the (C70)₂ dimer on its rovibrational spectroscopic properties: A theoretical survey. *J. Mol. Model.* **24**, 235 (2018).
39. Téllez, S. C. A., Pereira, L., Dos Santos, L., Fávero, P. & Martin, A. A. RM1 semi empirical and DFT: B3LYP/3-21G theoretical insights on the confocal Raman experimental observations in qualitative water content of the skin dermis of healthy young, healthy elderly and diabetic elderly women's. *Spectrochim. Acta Part A Mol. Biomol. Spectrosc.* **149**, 1009–1019 (2015).
40. Kim, K. H., Han, Y. K. & Jung, J. Basis set effects on relative energies and HOMO-LUMO energy gaps of fullerene C36. *Theor. Chem. Acc.* **113**, 233–237 (2005).
41. Ergürhan, O., Parlak, C., Alver, Ö. & Şenyel, M. Conformational and electronic properties of hydroquinone adsorption on C60 fullerenes: Doping atom, solvent and basis set effects. *J. Mol. Struct.* **1167**, 227–231 (2018).
42. Frisch, M. J. *et al.* Gaussian 09. 2009 (2009).
43. Chai, J. & Head-Gordon, M. Long-range corrected hybrid density functionals with damped atom–atom dispersion corrections. *Phys. Chem. Chem. Phys.* **10**, 6615 (2008).
44. Grimme, S. Semiempirical GGA-type density functional constructed with a long-range dispersion correction. *J. Comput. Chem.* **27**, 1787–1799 (2006).
45. Zhao, Y. & Truhlar, D. G. A new local density functional for main-group thermochemistry, transition metal bonding, thermochemical kinetics, and noncovalent interactions. *J. Chem. Phys.* **125**, 194101 (2006).
46. Boys, S. & Bernardi, F. The calculation of small molecular interactions by the differences of separate total energies: Some procedures with reduced errors. *Mol. Phys.* **19**, 553–566 (1970).
47. Singh, U. C. & Kollman, P. A. An approach to computing electrostatic charges for molecules. *J. Comput. Chem.* **5**, 129–145 (1984).
48. Bader, R. F. W. A quantum theory of molecular structure and its applications. *Chem. Rev.* **91**, 893–928 (1991).
49. Oliveira, B. G., Araújo, R. C. M. U. & Ramos, M. N. A topologia molecular QTAIM e a descrição mecânico-quântica de ligações de hidrogênio e ligações de di-hidrogênio. *Quim. Nova* **33**, 1155–1162 (2010).
50. Bader, R. F. W. & Essén, H. The characterization of atomic interactions. *J. Chem. Phys.* **80**, 1943 (1984).
51. Kumar, P. S. V., Raghavendra, V. & Subramanian, V. Bader's theory of atoms in molecules (AIM) and its applications to chemical bonding. *J. Chem. Sci.* **128**, 1527–1536 (2016).
52. Bader, R. F. W. *Atoms in Molecules: A Quantum theory* (Clarendon Press, 1990).
53. Contreras-García, J. *et al.* NCIPLOT: A program for plotting noncovalent interaction regions. *J. Chem. Theory Comput.* **7**, 625–632 (2011).
54. Johnson, E. R. *et al.* Revealing noncovalent interactions. *J. Am. Chem. Soc.* **132**, 6498–6506 (2010).
55. Gao, H. *et al.* Insights into the non-covalent interaction between modified nucleobases and graphene nanoflake from first-principles. *Phys. E Low-Dimensional Syst. Nanostruct.* **107**, 73–79 (2019).
56. Hernández-Paredes, J. *et al.* Experimental and theoretical study on the molecular structure, covalent and non-covalent interactions of 2,4-dinitrodiphenylamine: X-ray diffraction and QTAIM approach. *J. Mol. Struct.* **1141**, 53–63 (2017).
57. Thamotharan, S. *et al.* Quantitative analysis of intermolecular interactions in 2,2'-(4-bromophenyl)methylene)bis(3-hydroxy-5,5-dimethylcyclohex-2-en-1-one): Insights from crystal structure, PIXEL, Hirshfeld surfaces and QTAIM analysis. *J. Chem. Sci.* **130**, 20 (2018).
58. Lu, T. & Chen, F. Multiwfn: A multifunctional wavefunction analyzer. *J. Comput. Chem.* **33**, 580–592 (2012).
59. Humphrey, W., Dalke, A. & Schulten, K. V. M. D. Visual molecular dynamics. *J. Mol. Graph.* **14**, 33–38 (1996).
60. Hansen, P. L., Fallon, P. J. & Krätschmer, W. An EELS study of fullerite: C60/C70. *Chem. Phys. Lett.* **181**, 367–372 (1991).
61. Weaver, J. H. *et al.* Electronic structure of solid C60: Experiment and theory. *Phys. Rev. Lett.* **66**, 1741–1744 (1991).
62. Andreoni, W., Gygi, F. & Parrinello, M. Impurity states in doped fullerenes: C59B and C59N. *Chem. Phys. Lett.* **190**, 159–162 (1992).
63. Simeon, T. M., Yanov, I. & Leszczynski, J. Ab initio quantum chemical studies of fullerene molecules with substituents C 59X [X=Si, Ge, Sn], C 59X - [X=B, Al, Ga, In], and C 59X + [X=N, P, As, Sb]. *Int. J. Quantum Chem.* **105**, 429–436 (2005).
64. Li, F. *et al.* Theoretical study of hydrogen atom adsorbed on carbon-doped BN nanotubes. *Phys. Lett. Sect A Gen. At. Solid State Phys.* **357**, 369–373 (2006).
65. Varghese, S. S., Swaminathan, S., Singh, K. K. & Mittal, V. Ab initio study on gas sensing properties of group III (B, Al and Ga) doped graphene. *Comput. Condens. Matter* **9**, 40–55 (2016).
66. Dai, J., Yuan, J. & Giannozzi, P. Gas adsorption on graphene doped with B, N, Al, and S: A theoretical study. *Appl. Phys. Lett.* **95**, 232105 (2009).

67. Aihara, J. I. Reduced HOMO-LUMO gap as an index of kinetic stability for polycyclic aromatic hydrocarbons. *J. Phys. Chem. A* **103**, 7487–7495 (1999).
68. Bai, H. *et al.* Doping the buckminsterfullerene by substitution: Density functional theory studies of C₅₉X (X = B, N, Al, Si, P, Ga, Ge, and As). *J. Chem.* **2013**, 1–9 (2013).
69. Jing-Nan, L., Bing-Lin, G. & Ru-Shan, H. Electronic structures of doped fullerenes with boron and nitrogen atoms. *Solid State Commun.* **84**, 807–810 (1992).
70. Dunk, P. W. *et al.* Formation of heterofullerenes by direct exposure of C₆₀ to boron vapor. *Angew. Chem. Int. Ed.* **52**, 315–319 (2013).
71. Lu, J. *et al.* Structural and electronic properties of heterofullerene C₅₉P. *Mol. Phys.* **99**, 1203–1207 (2001).
72. Doust Mohammadi, M. & Abdullah, H. Y. Ab initio investigation for the adsorption of acrolein onto the surface of C₆₀, C₅₉Si, and C₅₉Ge: NBO, QTAIM, and NCI analyses. *Struct. Chem.* **33**, 363–378 (2022).
73. Paul, D., Deb, J. & Sarkar, U. A detailed DFT study on electronic structures and nonlinear optical properties of doped C₃₀. *ChemistrySelect* **5**, 6987–6999 (2020).
74. Silva, R. A. L., da Silva Filho, D. A., Moberg, M. E., Pappenfus, T. M. & Janzen, D. E. Halogen interactions in halogenated oxindoles: Crystallographic and computational investigations of intermolecular interactions. *Molecules* **26**, 5487 (2021).
75. Mohammadi, M. D., Salih, I. H. & Abdullah, H. Y. An ultimate investigation on the adsorption of amantadine on pristine and decorated fullerenes C₅₉X (X = Si, Ge, B, Al, Ga, N, P, and As): A DFT, NBO, and QTAIM study. *J. Comput. Biophys. Chem.* **20**, 23–39 (2021).
76. Slater, J. C. Atomic radii in crystals. *J. Chem. Phys.* **41**, 3199–3204 (1964).
77. Javan, M. B. & Ganji, M. D. Theoretical investigation on the encapsulation of atomic hydrogen into heterofullerene nanocages. *Curr. Appl. Phys.* **13**, 1525–1531 (2013).
78. Shariatnia, Z. & Shahidi, S. A DFT study on the physical adsorption of cyclophosphamide derivatives on the surface of fullerene C₆₀ nanocage. *J. Mol. Graph. Model.* **52**, 71–81 (2014).
79. Etmnan, N., Yoosefian, M., Raissi, H. & Hakimi, M. Solvent effects on the stability and the electronic properties of histidine/Pd-doped single-walled carbon nanotube biosensor. *J. Mol. Liq.* **214**, 313–318 (2016).
80. Behjatmanesh-Ardakani, R., Pourroustaei-Ardakani, F., Taghdiri, M. & Kotena, Z. M. DFT-B3LYP study of interactions between host biphenyl-1-aza-18-crown-6 ether derivatives and guest Cd²⁺: NBO, NEDA, and QTAIM analyses. *J. Mol. Model.* **22**, 149 (2016).
81. Tariq, S. *et al.* Experimental and computational investigations of new indole derivatives: A combined spectroscopic, SC-XRD, DFT/TD-DFT and QTAIM analysis. *J. Mol. Struct.* **1207**, 127803 (2020).

Acknowledgements

This work was funded by Conselho Nacional de Desenvolvimento Científico e Tecnológico (CNPq) and Coordenação de Aperfeiçoamento Pessoal de Nível Superior (CAPES), and Fundação de Apoio à Pesquisa do Distrito Federal (FAP-DF), and Fundação de Amparo à Pesquisa do Estado de Goiás (FAPEG).

Author contributions

R.A.L.S., L.R. and D.A.S.F. designed the project, R.A.L.S., D.F.S.M. and H.C.B.O. performed the data analysis. R.A.L.S., D.F.S.M. and H.C.B.O. wrote the manuscript. R.A.L.S., D.A.S.F. and L.R. carried out the calculations.

Competing interests

The authors declare no competing interests.

Additional information

Supplementary Information The online version contains supplementary material available at <https://doi.org/10.1038/s41598-022-19258-6>.

Correspondence and requests for materials should be addressed to R.A.L.S.

Reprints and permissions information is available at www.nature.com/reprints.

Publisher's note Springer Nature remains neutral with regard to jurisdictional claims in published maps and institutional affiliations.



Open Access This article is licensed under a Creative Commons Attribution 4.0 International License, which permits use, sharing, adaptation, distribution and reproduction in any medium or format, as long as you give appropriate credit to the original author(s) and the source, provide a link to the Creative Commons licence, and indicate if changes were made. The images or other third party material in this article are included in the article's Creative Commons licence, unless indicated otherwise in a credit line to the material. If material is not included in the article's Creative Commons licence and your intended use is not permitted by statutory regulation or exceeds the permitted use, you will need to obtain permission directly from the copyright holder. To view a copy of this licence, visit <http://creativecommons.org/licenses/by/4.0/>.

© The Author(s) 2022